Available online at www.sciencedirect.com
SCIENCE DIRECT®
Earth and Planetary Science Letters 241 (2006) 888–900
EPSL
www.elsevier.com/locate/epsl

# Scattering coefficients in the mantle revealed from the seismogram envelope analysis based on the multiple isotropic scattering model

Won Sang Lee [a,*], Haruo Sato [a], Kiehwa Lee [b]

[a] *Department of Geophysics, Graduate School of Science, Tohoku University, Sendai, Japan*
[b] *Seismological Observatory, School of Earth and Environmental Sciences, Seoul National University, Seoul, Republic of Korea*

Received 29 March 2005; received in revised form 24 October 2005; accepted 25 October 2005
Available online 1 December 2005
Editor: R.D. van der Hilst

**Abstract**

At longer periods, scattered ScS waves sometimes dominate over coda waves at large lapse times. Examining recordings of seismic envelopes at 9 IRIS seismic stations of regional earthquakes with focal depths deeper than 150 km in periods from 1 to 20 s for a wide lapse time range up to 2000 s, we found significant frequency dependence. The coda decay gradient at short periods is steeper than that at longer periods; however, the change of coda gradient associated with the ScS arrival becomes distinct as the period becomes longer. In particular, a clear offset of coda amplitude appears in central Asia for 10 and 15 s period bands. The multiple isotropic scattering process of S-waves in the heterogeneous mantle can be simply simulated by using the Monte Carlo simulation method based on the radiative transfer theory in scattering media. Assuming a two-plane-layer attenuation structure and smoothed velocity model of the PREM, we estimated the average total scattering coefficients of S-waves such as $7.52\times10^{-4}$~$1.32\times10^{-3}$ km$^{-1}$ and $2.08\times10^{-4}$~$6.23\times10^{-4}$ km$^{-1}$ at 4 s, and $4.51\times10^{-4}$~$7.37\times10^{-4}$ km$^{-1}$ and $2.80\times10^{-5}$~$2.71\times10^{-4}$ km$^{-1}$ at 10 s, for the lithosphere and the upper mantle and for the lower mantle, respectively. Our results indicate that scattering occurs mostly in the lithosphere and the upper mantle and support that medium heterogeneity spreads over the whole mantle though its scattering power is small. Strong scattering occurs beneath central Asia and Papua New Guinea, whereas the scattering beneath Italy and regions of east Russia is much weaker. The numerical calculation enables us to confirm that much stronger scattering than intrinsic attenuation causes the offset behavior with coda decay gradient change after the ScS arrival for 4 and 10 s period bands in some regions.


*Keywords:* ScS; coda; mantle heterogeneity; radiative transfer theory; total scattering coefficient; multiple isotropic scattering

## 1. Introduction

Coda waves are considered to be composed of incoherent waves scattered by distributed heterogeneities in the Earth medium. The coda energy propagation is generally modeled with statistical scattering theories based on random media models. The excitation level of coda waves and the temporal decay gradient of coda amplitudes are the most important data for quantifying the scattering strength and attenuation of the real Earth medium.

Coda attenuation $Q_C^{-1}$ characterizes the seismogram coda amplitude decay with lapse time, and total scattering $g_0$ is defined as the average of the scattering coefficient over all directions in heterogeneous media. There have been a lot of measurements of coda atten-

* Corresponding author. Tel.: +81 22 795 6533; fax: +81 22 795 6783.
*E-mail address:* lee@zisin.geophys.tohoku.ac.jp (W.S. Lee).

0012-821X/$ - see front matter © 2005 Elsevier B.V. All rights reserved.
doi:10.1016/j.epsl.2005.10.035

uation $Q_C^{-1}$ and total scattering coefficients of S-wave $g_0$ in the world [1]. In general, $Q_C^{-1}$ is about $10^{-2}$ at 1 Hz and decreases to about $10^{-3}$ at 20 Hz, and $g_0$ for S-to-S wave scattering is of the order of $10^{-2}$ km$^{-1}$ for frequencies 1–30 Hz. Most previous studies of coda, however, have been done for lapse times shorter than a few hundred seconds and for periods shorter than 1 s even though there are some exceptions [2–4]. Most studies have been focused on characterizing the heterogeneity of the lithosphere.

Resolving the location and characteristics of the scatterers is important because they provide some of the best constraints on the distribution of small-scale (tens of kilometers or less) heterogeneity to understand the nature of mantle convection in the deep Earth. A deterministic approach to resolve small-scale heterogeneity is not suitable because seismic tomography, which averages over large volumes in the lower mantle, cannot resolve heterogeneities smaller than hundreds of kilometers in size with present techniques. On the contrary, a statistical characterization of its properties can be made from observations of the scattered wavefield. The high-frequency coda following from direct P and S arrivals is an example of such a scattered wavefield, and studies of seismic coda have led to a number of advances in scattering theory and in the characterization of crustal heterogeneity and attenuation. However, it is difficult to use P and S coda observations to constrain the distribution of small-scale heterogeneity in the deep mantle and core because of the uncertainties involved in removing the strong scattering signal contributed by the crust and uppermost mantle.

Recently, several studies have investigated the mantle heterogeneity and suggest that small-scale medium heterogeneity exists not only in the vicinity of the core–mantle boundary (CMB) but in the whole lower mantle revealed from the analysis of PKP precursors [5–8], global P coda [9], $P_{diff}$ [10] coda and ScS coda [11]. Hedlin et al. [5] proposed that the global average small-scale heterogeneity has a scale length of about 8 km with P wave RMS velocity fluctuation of 1%, and Margerin and Nolet [7,8] and Shearer and Earle [9] explained PKP precursor amplitudes using a model with a 0.1–0.5% velocity fluctuation. The study of mantle heterogeneity is quite an important issue in seismology as well as other Earth sciences.

The core–mantle reflected phase ScS is clearly shown in long period seismograms, and an offset behavior in coda decay sometimes appears around ScS arrival particularly in central Asia [11]. For a preliminary survey, we examined and systematically classified global seismic envelopes for a wide period range from 1 to 20 s, for lapse-times as long as 2000 s, and the result suggested that the coda decay rate changes from before to after the ScS arrival and may reflect the regional variation of medium heterogeneity in the mantle and the roughness of the CMB region. Lee et al. [11] indicated the frequency dependence of envelope characteristics associated with the ScS arrival such as the change of coda decay gradient around the ScS arrival becomes smaller with increasing frequency and proposed that envelope characteristics before and after the ScS arrivals could be a good indicator to measure the average strength of medium heterogeneity in the mantle region. Moreover, they found much stronger scattering than intrinsic attenuation beneath central Asia from using the direct simulation Monte Carlo (DSMC) method [12] based on the radiative transfer theory for isotropic scattering process of S-waves.

In this study, we estimate the range of the average total scattering coefficients in the lithosphere and the mantle regions, and show regional variation of the values over the world by examining the coda decay characteristics of regional earthquakes recorded at 9 IRIS seismic stations. We assume a two-plane-layer attenuation model and use the simulation technique of Lee et al. [11], which is based on the DSMC method [12] for synthesizing the MS envelopes to estimate the total scattering coefficient in the mantle. The decay of coda envelopes was investigated in several period bands from 1 to 20 s for lapse times as long as 2000 s. This lapse time range includes ScS and $ScS_2$ arrivals for regional earthquakes.

## 2. Data and observation

### 2.1. Data selection

We use broadband NS-component velocity seismograms of regional earthquakes recorded by the IRIS seismic network stations, which is well distributed over the world. These digital data have 20 Hz sampling and are suitable for the study of envelopes around the ScS arrivals in the period range from 1 to 20 s. Since the surface waves are sometimes dominant even after ScS arrivals for events with focal depth less than 50 km [11], we selected earthquakes deeper than 150 up to 680 km in depth to avoid being severely contaminated by surface waves in the period band from 1 to 20 s, and we extend the study area to the entire world. Accordingly, we collected 61 events recorded at 9 IRIS seismic stations during the period between 1992 and 2004 with epicentral distances less than 1500 km from individual stations and moment magnitudes ($M_W$) between

5.1 and 7.2 (Fig. 1) in order to measure the range of the average total scattering coefficients in the lithosphere and the mantle, and investigate spatial variation of the values in the world.

### 2.2. Making MS envelopes

To characterize the S-coda envelopes we often calculate the smoothed trace of the square of the seismogram, which is called the mean square (MS) seismogram envelope. The MS envelope, whose amplitude is linearly proportional to energy density, is appropriate for comparison with the synthesis based on the radiative transfer theory.

Fourth-order Butterworth band-pass filters having center periods of 1, 2, 4, 10, 15 and 20 s are applied to data. The bandwidth of each band-pass filter is 2/3 of the inverse of the center period. Smoothing the square of band-pass filtered trace with a time constant of each center period, we compute MS envelope traces. As an example, Fig. 2 shows the logarithm of the MS band-pass filtered envelopes from 1 to 20 s period bands at EKS2 in central Asia for 7 earthquakes located less than 800 km from the station. To correct the source–size differences, we normalized each trace by the average coda level at lapse time ranging from 650 to 750 s as marked by a bold solid bar at the bottom of the figure. The theoretical S and ScS arrivals of the average epicentral distance and focal depth for the observed events calculated from the *iasp91* model [13] are drawn by dashed lines. Gray traces are normalized MS envelopes from 7 regional earthquakes, and black ones are stacked MS envelopes for each period band. The change of coda slopes seems to be initiated from about 750 s. It is presumed to be primarily related to the stacking technique which does not take a 'delay and sum' procedure into account. That is, such an artifact could be caused by the fluctuation of ScS arrivals. As shown in the figure, at 1, 2 and 4 s periods, the decay gradient is smooth irrespective of the ScS arrival and there is little change in envelope slope around ScS arrival. At 10, 15 and 20 s periods, however, the ScS phase clearly appears, the envelope decay gradients are different before and after the ScS arrival, and there is an offset of the envelope level around the ScS arrival. Lee et al. [11] reported frequency dependence of the coda envelope decay curves in the period bands.

## 3. Numerical modeling

### 3.1. Monte Carlo simulation

The analysis of S-wave envelopes of local and regional earthquakes is one of the most effective strategies for investigating the heterogeneous Earth structure characterized by seismic scattering and attenuation. To examine the attenuation mechanism in the lithosphere and the mantle using the analysis of S-wave coda at large lapse time, we synthesize seismogram envelopes for deep focus (deeper than 150 km in depth) regional earthquakes using the Monte Carlo simulation method.

The radiative transfer theory has been an attractive theory since it allows relatively tractable calculations of the effects of multiple scattering even though it is phenomenological. Furthermore, the radiative transfer approach forms the basis of a practical analysis method to estimate the amount of scattering caused by intrinsic

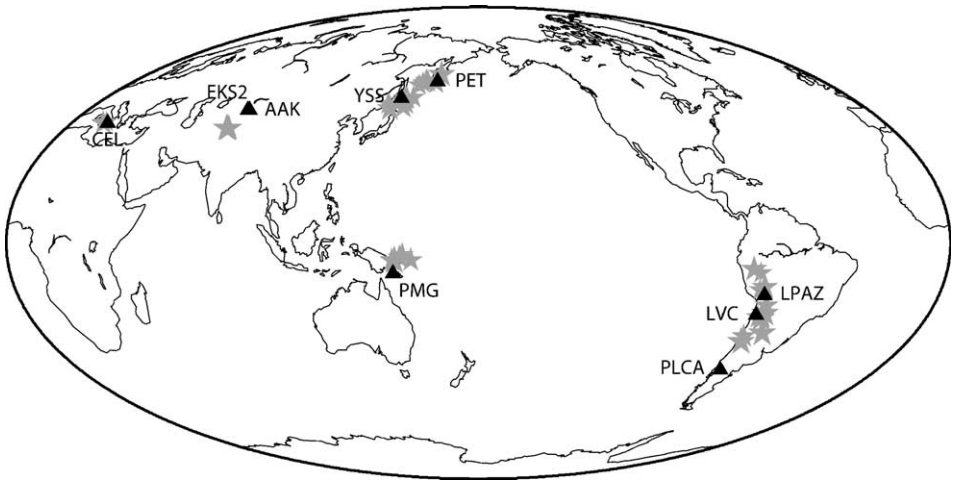


Fig. 1. Location of 9 IRIS seismic stations (triangles) and 61 events (stars) of deep focus earthquakes used in this study.

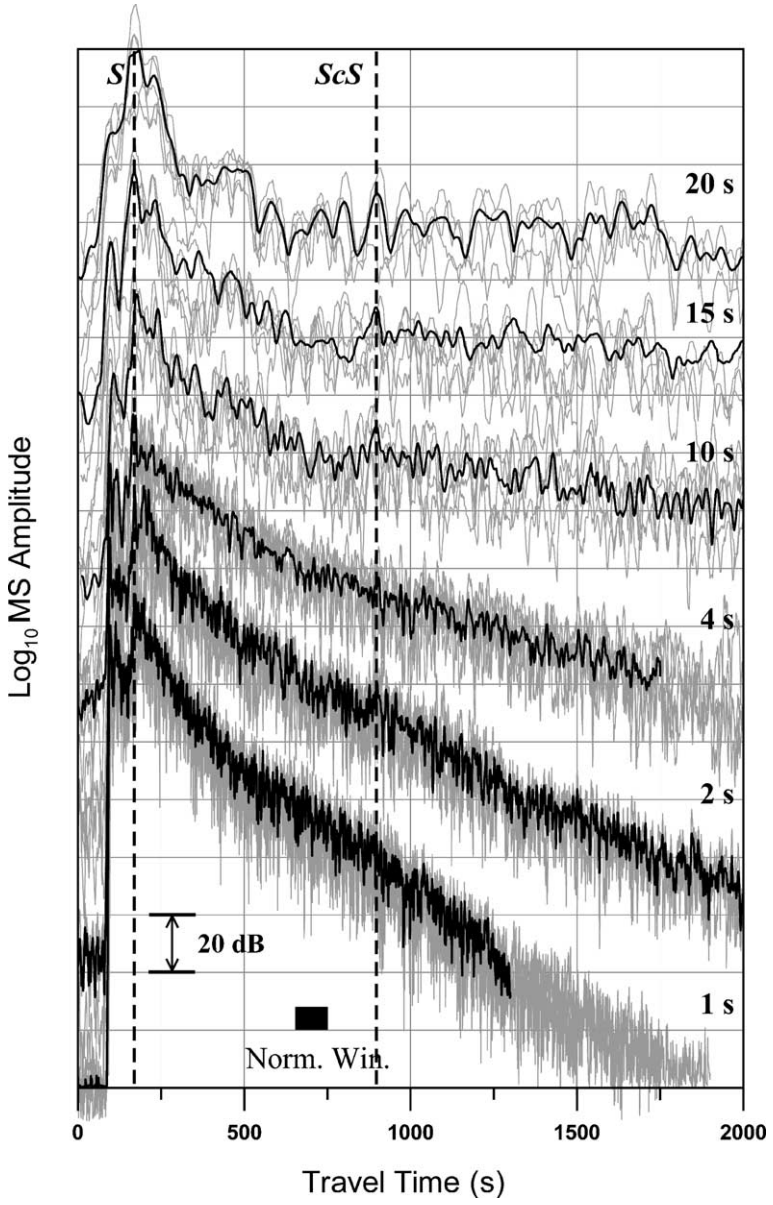


Fig. 2. Plots of the logarithm of the MS band-pass filtered envelopes from 1 to 20 s period bands at EKS2 in central Asia. Gray traces are for 7 regional earthquakes within 800 km epicentral distances and 250 km in depths. MS envelopes of each period band are normalized by coda amplitude at lapse time ranging from 650 to 750 s as indicated by a bold bar at the bottom. Black traces are stacked MS envelopes. Vertical dashed lines indicate theoretical S and ScS arrivals of the average epicentral distance and focal depth for the observed events according to the *isap91* model.

and scattering mechanisms. The Monte Carlo simulation method, which is based on the analogy between radiative transfer theory and the Boltzmann equation in the kinetic theory of gases [14], is well known as a useful and popular technique to simulate seismic envelopes in randomly distributed scattering media and plays an important role in investigating the effect of velocity structure on coda envelopes. The propagation of energy is represented by the movement of a large number of energy particles in the simulation method. Applying an analytical integral representation for the distance between scattering points, Hoshiba [15] developed an efficient algorithm for a simple structure model and studied the characteristics of coda envelopes in layered media. For the numerical simulation of a realistic Earth model with irregular seismic velocities, we use a direct simulation Monte Carlo (DSMC) method developed by Yoshimoto [12] in this study. The DSMC method which

utilizes a finite difference scheme for ray tracing, has an advantage over previous methods in terms of flexibility, and can be applied to three dimensional velocity structures. We assume a depth-dependent three dimensional random distribution of point-like isotropic scatterers and a background S-wave propagation velocity $V_S$ which is adopted by the Preliminary Reference Earth Model (PREM) [16] with a slight modification to evaluate the effect of seismic ray bending on coda envelopes in each plane layer.

In general, scattering pattern has several lobes and generally stronger in the forward direction. Therefore, the isotropic scattering model cannot precisely explain the detailed envelope near the direct arrival. The isotropic scattering model, however, still works in describing quantitatively coda envelopes, where the total scattering coefficient $g_0$ is related with the transport scattering coefficient of waves in random media [17,18]. It presents the effective isotropic scattering coefficient.

### 3.2. Test of DSMC method

In this section, we examine the validity and stability of the DSMC method for application to the complex velocity structure down to the core–mantle boundary (CMB) since the method has previously been used for only the analysis of heterogeneous lithospheric structure. First, we compare synthetic seismograms obtained by the DSMC method for an isotropic scattering process in a three dimensional scattering media with the analytic solution for the single-scattering model. Then, we simulate seismic envelopes using the DSMC method in media with varying total scattering coefficients ($g_0$), which governs the strength of S-coda excitation [1], for each layer. Quantity $g_0$ has dimension of reciprocal length. Finally, assuming a two-plane-layer attenuation structure, we investigate the influence of $g_0$ in each layer.

#### 3.2.1. Comparison with analytic solution

We assume two cases for making seismogram envelopes using the DSMC method as follows:

1. Half space medium: Seismic wave is totally reflected at the surface and there is no seismic boundary at the bottom.
2. One layer medium: Seismic wave is totally reflected at the surface and the bottom of a layer (CMB).

The global parameters used in the numerical simulation are listed in Table 1. Analytic solution of the single-scattering model in infinite three-dimensional medium is [1]

$$E^1(\mathbf{x},t) = \frac{W g_0}{2\pi V_S^2 t^2} \exp\left(-Q_C^{-1} 2\pi f t\right) \quad (1)$$

where $E^1$ is the energy density for single scattering and $Q_C^{-1}$ is easily given by $Q_C^{-1}(f) = Q_i^{-1}(f) + g_0 V_S / 2\pi f$. We introduce intrinsic attenuation, $Q_i$, as 1000 that was proposed by Hoshiba [19] for depths greater than 100 km.

Table 1
Global parameters used in the DSMC for comparison with analytic solution

| | |
|---|---|
| $g_0$ (km$^{-1}$) | $10^{-5}$ |
| $Q_i$ | 1000 |
| $V_S$ (km/s) | 6 |
| Time interval (s) | 1 |
| Duration (s) | 2000 |
| Number of particles | $10^8$ |
| Source depth (km) | 15 |
| Epicentral distance (km) | 200 |
| Depth of the bottom layer (km) | 2890 |
| Radius of receiver volume (km) | 6 |
| Predominant period (s) | 10 |

For the first and the second cases of the numerical simulation, the DSMC results show the seismic energy exponentially decreases monotonously with increasing lapse time. In Fig. 3(a), the energy density from the analytic solution is multiplied by two. Practically the value for the half space medium is twice for the infinite medium. They are in quite good agreement with the analytic solution for single-scattering model since the lapse time is shorter than the mean free time 100,000/6 s (Fig. 3a). For the second case (Fig. 3b) of the simulation, the offset behavior in the envelope appears after the ScS arrival as we discovered.

#### 3.2.2. Depth dependence of total scattering coefficient

The total scattering coefficient has been shown to decrease with increasing lapse time $t$ [20]. In other words, the total scattering coefficient decreases with depth. In this section, we introduce a simple two layered attenuation structure (still the uniform velocity structure) to numerical simulation.

The simulation parameters are enumerated for each case in Table 2. The thickness of the upper layer is 200 km and the depth of the bottom layer is 2890 km. The period is 10 s for cases 1, 2 and 3 (Fig. 4a), and is 1 s for cases 4, 5 and 6 (Fig. 4b). For 1 s period band, the coda envelopes rapidly decrease with increasing lapse time as we observed. As seen in Fig. 4, we can find that the coda amplitude becomes much excited and the ScS

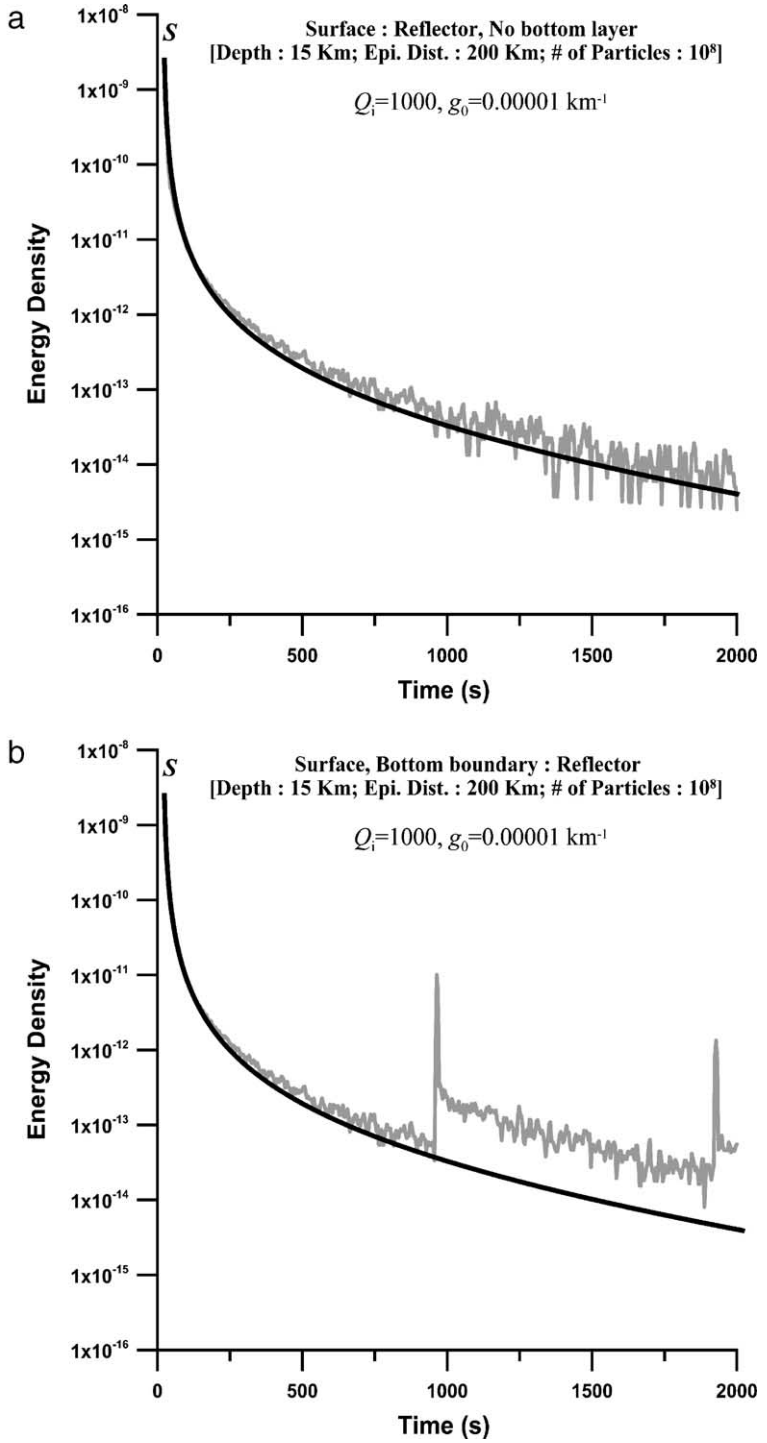


Fig. 3. A comparative plot of envelopes for the DSMC result and analytic solution. (a) Half space medium; total reflection at the surface. (b) One layer medium; total reflection at the surface and the bottom of layer. Gray traces and black curves represent the DSMC result and the analytic solution, respectively. The numerical simulation is in good agreement with the analytic solution. In the second case, (b), ScS and $ScS_2$ phases appear and an offset behavior is shown after the ScS arrival.

Table 2
Depth dependent attenuation structures considered in the Section 3.2.2

| Case | Thickness of upper layer (km) | $g_0$ upper layer ($km^{-1}$) | $g_0$ lower layer ($km^{-1}$) | $Q_i$ both layers | Predominant period (s) | Time interval (s) |
|---|---|---|---|---|---|---|
| 1 | 200 | 0.0001 | 0.0001 | 1000 | 10 | 1 |
| 2 | 200 | 0.001 | 0.0001 | 1000 | 10 | 1 |
| 3 | 200 | 0.01 | 0.0001 | 1000 | 10 | 1 |
| 4 | 200 | 0.0001 | 0.0001 | 1000 | 1 | 1 |
| 5 | 200 | 0.001 | 0.0001 | 1000 | 1 | 1 |
| 6 | 200 | 0.01 | 0.0001 | 1000 | 1 | 1 |

S-wave velocity: 6 km/s.
Source depth: 15 km.
Epicentral distance: 200 km.
Depth of bottom layer: 2890 km.
Number of particles: one million.

arrival embedded in coda waves with increasing $g_0$ for the upper layer. Although the simulation is performed under very simple conditions, the simulations demonstrate that the DSMC method could produce stable and reasonable results to analyze the observed envelopes.

### 3.3. Velocity and attenuation structure

The treatment of seismic waves is completely scalar in this study by neglecting conversion scattering between P and S waves and scattering is assumed to be isotropic. In the simulation, we have the total scattering coefficient $g_0$ changed based on the modified PREM model [11] (Fig. 5) and assume that the source radiation is isotropic.

We use the background S-wave velocity structure having a positive gradient with depth as illustrated in Fig. 5. According to the PREM, total attenuation profile chosen mostly from body wave studies can be approximated by a two-plane-layer model where the boundary is 670 km in depth, where we neglect the narrow low $Q$ zone at 80–220 km in depth; $Q_\mu$ (total attenuation) values of the upper layer (Layer 1) and the lower layer (Layer 2) are 143 and 312, respectively (see a broken line in Fig. 5). The total attenuation consists of scattering loss and intrinsic absorption. The scattering power is given by the total scattering coefficient $g_0$ for each period. Total attenuation $Q_\mu$ provides a strong constraint for the range of variation of $g_0$. When the total scattering coefficient is given, the intrinsic attenuation term can be easily calculated by the relationship

$$\frac{1}{Q_i(f)} = \frac{1}{Q_\mu} - \frac{g_0 V_S}{2\pi f} \quad (2)$$

for a given depth and central frequency $f$ in Hz.

In the DSMC modeling, we adopt a time step of $\Delta t(f) = 0.2/f$ in seconds, which is roughly less than one hundredth of mean free time $(1/g_0(f)V(z))$. One million particles are shot from the source. The number of energy particles contained in a receiver volume is binned into 10 s intervals. At the free surface and the CMB we assume total reflection. And for simplicity, reflection from the transition structure that includes a discontinuity of the first derivative of velocity is not considered in the synthesis. We put the source at the average depth of events analyzed at each station to make synthetic seismogram envelopes. Since deep sources greater than 150 km in depth were selected, we consider upgoing as well as downgoing rays in the simulation. Thus we can find the depth phase such as sScS after ScS arrival in the synthetics. In the observation data, however, the depth phase sScS is not quite visible since sScS has been more attenuated than ScS because of longer propagation distance. By using geometrical symmetry with respect to the epicenter we used a torus volume just beneath the free surface having a semicircle section to count the number of energy particles at a receiver. The radius of the semicircle is chosen to be 3.2 (km/s) × time interval (s).

## 4. Estimation of total scattering coefficient

For a medium filled with randomly distributed scatterers, the scattering power per unit volume is given by the product of the number density and the differential scattering cross-section, which is called the scattering coefficient [21].

We analyze stacked NS-component broadband velocity seismograms of the regional earthquakes registered by 9 stations of the IRIS to estimate the total scattering coefficient using the DSMC method for 1, 2, 4, 10, 15 and 20 s period bands. There is practically no significant difference for the stacked seismogram envelopes between NS- and EW-components on the coda

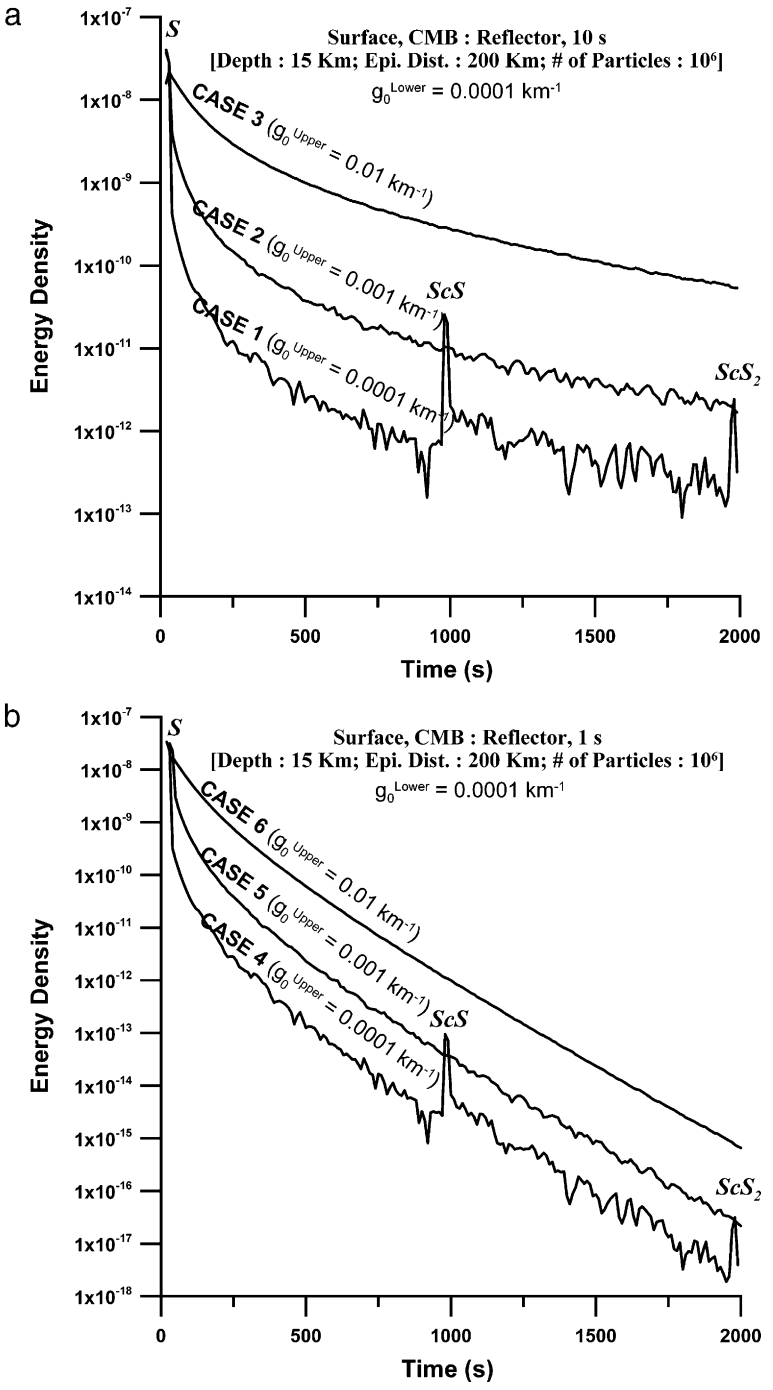


Fig. 4. Envelopes for depth dependence of total scattering coefficient in the two-layer model. The thickness of the upper layer is 200 km and the depth of bottom layer is 2890 km. (a) Envelopes for 10 s, (b) envelopes for 1 s. Coda level increases with increasing the scattering coefficient for the upper layer. The coda decay gradient of cases 4, 5 and 6 (1 s) is much steeper than that of cases 1, 2 and 3 (10 s). See Table 2 for the simulation parameters in detail.

portion. To correct the source-size differences, we plot these traces normalizing the average coda level at lapse time ranging from 650 to 750 s. The velocity and attenuation model, simulation parameters and assumptions are identical with the method ensured in the previous sections.

In order to assess the best agreement between a particular model and the observations, we use

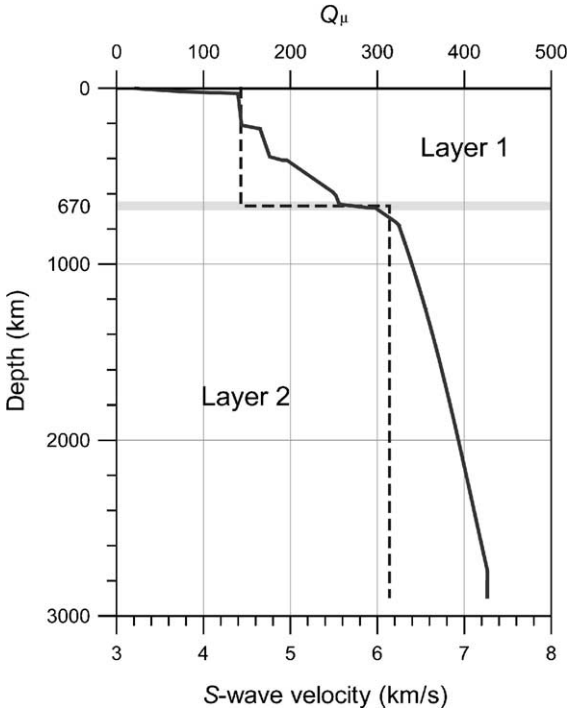


Fig. 5. The velocity structure (solid line) and the attenuation structure (dashed line) used in the synthesis. The velocity structure is modified after the PREM model for S-wave velocity. We use a two-layer scattering model for scattering and attenuation, where total attenuation $Q_\mu$ values of Layer 1 (shallower than 670 km in depth) and Layer 2 (up to the CMB) are 143 and 312, respectively.

a simple $\chi^2$ fitting method, where $\chi^2$ is defined as

$$\chi^2 = \frac{1}{N}\sum_{i=1}^{N}\left(\frac{d(t_i) - y\left(g_0^{\text{Layer1}}, g_0^{\text{Layer2}}, t_i\right)}{\sigma(t_i)}\right)^2. \qquad (3)$$

Here, $d(t_i)$ is the observed logarithmic MS amplitude at time $t_i$, $y(g_0^{\text{Layer1}}, g_0^{\text{Layer2}}, t_i)$ is the modeled logarithmic energy density for a given value of the total scattering coefficients ($g_0^{\text{Layer1}}$ and $g_0^{\text{Layer2}}$) for the upper and the lower layers, $\sigma$ is a typical uncertainty of the measurements, and the sum runs over all data points in the time window ranging between 500 and 1500 s except for the data of LPAZ at 4 s. We carried out a grid search analysis to seek a pair of parameters ($g_0^{\text{Layer1}}, g_0^{\text{Layer2}}$) that minimizes $\chi^2$ value. In the grid search analysis, the maximum and the minimum boundary values of $g_0(f)$ are 98% and 2% of $g_{0\mu}(f)$ calculated from $Q_\mu$ for each layer in the simulation.

The resultant total scattering coefficients for Layer 1 and Layer 2 range as follows; $7.52\times10^{-4}$~$1.32\times10^{-3}$ km$^{-1}$ and $2.08\times10^{-4}$~$6.23\times10^{-4}$ km$^{-1}$ at 4 s, and $4.51\times10^{-4}$~$7.37\times10^{-4}$ km$^{-1}$ and $2.80\times10^{-5}$~$2.71\times10^{-4}$ km$^{-1}$ at 10 s, respectively (Table 3). Some regional differences in lower mantle are indicated, such as strong scattering beneath central Asia (4 and 10 s) and Papua New Guinea (4 s) and weak scattering beneath Italy (10 s) and regions of east Russia (10 s). In Fig. 6, we show the stacked observation data by gray traces and the best-fit synthetic envelopes by black traces for the period bands 4 and 10 s for each station. The vertical thick gray line indicates the range of the ScS arrival, and the right-most panel presents the relative residual, which is normalized by the largest residual, in grid search analysis for each period band between 9 stations. That is, the total scattering coefficients at LPAZ and AAK for 4 s and at AAK and YSS for 10 s are much more reliable than those of other stations.

Fig. 6 exhibits good coincidence between the observed data and the synthetic envelopes except lapse time around 250 s for 10 s period. The discrepancy before 250 s could be explained by the influence of the surface waves in the 10 s period band. We can find a small offset with small coda decay gradient for 4 s and a clear offset with the big change of coda decay gradient

Table 3
Estimated total scattering coefficients ($g_0$) and seismic Albedo ($B_0$) for 9 IRIS seismic stations

| Station | 4 s | | | | 10 s | | | |
|---|---|---|---|---|---|---|---|---|
| | Layer 1 | | Layer 2 | | Layer 1 | | Layer 2 | |
| | $g_0$ (km$^{-1}$) | $B_0$ | $g_0$ (km$^{-1}$) | $B_0$ | $g_0$ (km$^{-1}$) | $B_0$ | $g_0$ (km$^{-1}$) | $B_0$ |
| CEL | – | – | – | – | $7.37\times10^{-4}(\pm10\%)$ | 54–98% | $8.30\times10^{-5}(\pm10\%)$ | 24–30% |
| AAK | $1.13\times10^{-3}(\pm20\%)$ | 33–60% | $6.23\times10^{-4}(\pm20\%)$ | 72–90% | $4.51\times10^{-4}(\pm10\%)$ | 33–60% | $2.71\times10^{-4}(\pm10\%)$ | 79–98% |
| EKS2 | $1.13\times10^{-3}(\pm20\%)$ | 33–60% | $6.23\times10^{-4}(\pm20\%)$ | 72–90% | $4.51\times10^{-4}(\pm10\%)$ | 33–60% | $2.22\times10^{-4}(\pm10\%)$ | 64–80% |
| YSS | $1.13\times10^{-3}(\pm20\%)$ | 33–60% | $6.23\times10^{-4}(\pm20\%)$ | 72–90% | $6.77\times10^{-4}(\pm10\%)$ | 49–90% | $2.80\times10^{-5}(\pm10\%)$ | 8–10% |
| PET | $1.32\times10^{-3}(\pm20\%)$ | 38–70% | $2.08\times10^{-4}(\pm20\%)$ | 24–30% | $6.77\times10^{-4}(\pm10\%)$ | 49–90% | $2.80\times10^{-5}(\pm10\%)$ | 8–10% |
| PMG | $9.40\times10^{-4}(\pm20\%)$ | 27–50% | $5.54\times10^{-4}(\pm20\%)$ | 64–80% | – | – | – | – |
| LPAZ | $7.52\times10^{-4}(\pm20\%)$ | 22–40% | $2.08\times10^{-4}(\pm20\%)$ | 24–30% | $5.27\times10^{-4}(\pm10\%)$ | 38–70% | $2.71\times10^{-4}(\pm10\%)$ | 79–98% |
| LVC | – | – | – | – | $6.77\times10^{-4}(\pm10\%)$ | 49–90% | $1.94\times10^{-4}(\pm10\%)$ | 56–70% |
| PLCA | $9.40\times10^{-4}(\pm20\%)$ | 27–50% | $4.16\times10^{-4}(\pm20\%)$ | 48–60% | – | – | – | – |

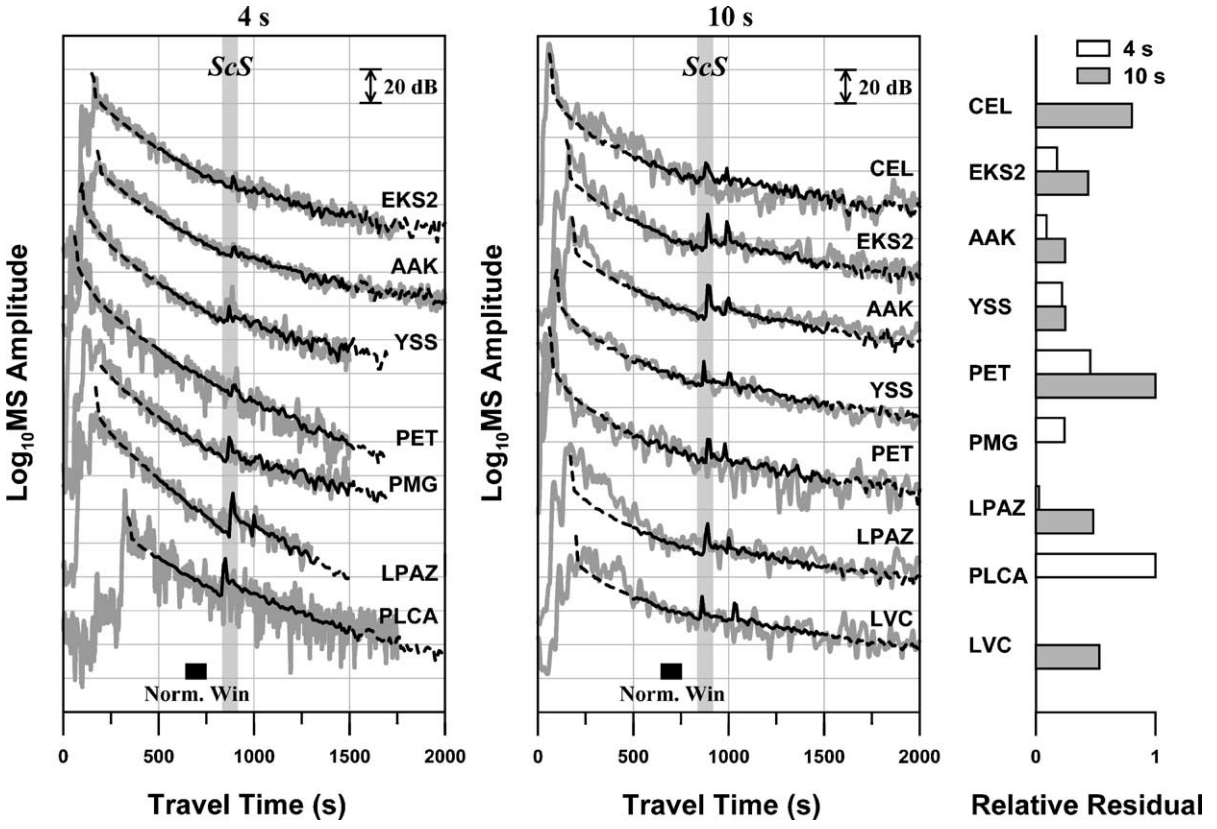


Fig. 6. The best fits between the envelope stack for deep focus (≥150 km) events and the simulated envelope applied to the radiative transfer theory. The MS envelopes are normalized coda amplitude at lapse times from 650 to 750 s as indicated by a bold bar at the bottom. Gray curves show the observed stack envelopes for 4 and 10 s period bands registered by 9 IRIS seismic stations. The best-fit synthetic MS envelopes are represented by black curves. The target window for the grid search analysis is from 500 to 1500 s in lapse time (LPAZ for 4 s is up to 1300 s) drawn by solid black curves. The right-most panel, the relative residual calculated from the minimum $\chi^2$ for each station, shows relative reliability of the estimated total scattering coefficients for 4 and 10 s. White and gray bars are for 4 and 10 s, respectively.

for 10 s after the ScS arrival in the simulation at some stations. Since the influence of the surface waves is too strong in observed data for period bands of 15 and 20 s, our S-wave scattering model is hardly able to simulate surface wave scattering. For 1 and 2 s period bands, the synthetic envelopes based on a two-layer scattering model are not proper to explain simultaneously the strong ScS peak and the smooth decay of envelopes.

In Fig. 6, we can find that the falloff slopes at 4 s are steeper than those at 10 s, corresponding to greater scattering values in Table 3. This relationship, however, appears reversed when comparing the values for individual stations at a given period band. For example, at 4 s, the LPAZ falloff is clearly steeper than the falloff of PLCA, yet the scattering values in Table 3 show less scattering. Generally speaking, greater scattering strength produces less steep decay gradient in seismic envelopes at a given period band since more scattered energy could be easily come back. Therefore, it is quite reasonable that the total scattering coefficient of PLCA is greater than that of LPAZ at 4 s. In the case of comparison for different periods, seismic energy of short period bands would be more attenuated than that of longer period bands although the heterogeneous media have the same scattering coefficient since intrinsic attenuation is governed by Eq. (2) in the simulation (Fig. 4). Consequently, it is difficult to simply compare the scattering strength from just considering the falloff slopes for different period bands.

## 5. Discussion

In general, since scattering is much stronger near the Earth's surface than deeper in the mantle, the ScS phase is unclear in short-period seismograms. Attenuation of seismic energy is caused by intrinsic absorption and depends on the predominant frequency. Scattering attenuation, however, contributes redistribution of seismic wave energy. In the numerical modeling, supposing an attenuation factor $AF(f)=\exp(-2\pi f\Delta t/Q_i)$ for time step

$\Delta t$, where $Q_i$ is obtained by Eq. (2), and seismic energy $E(t+\Delta t)=E(t)\times AF(f)$, the energy of 4 s is more attenuated than that of 10 s in both upper and lower layers. Thus, the ScS phase is less visible at shorter period bands. And much longer propagation distance of ScS phase compared to direct S phase causes more attenuated amplitude of ScS than direct S. Moreover, as we assume the reflectivity of the CMB as 1, that is total reflection, and simulate the seismic envelopes under very small total scattering coefficients, the ScS arrivals appear all synthetics. However, if we introduce somewhat stronger total scattering coefficient to the upper layer, the change of decay gradient and offset behavior becomes unclear as shown in Fig. 4. We will consider the influence of reflectivity into the simulation in near future.

Aki and Chouet [21] and Rautian and Khalturin [2] concluded that coda waves of periods longer than 1 s were thought to be mostly composed of scattered surface waves. In this study, however, we showed that envelopes of deep focus earthquakes at lapse times longer than about 1000 s are mostly composed of scattered S-waves associated with the ScS arrival rather than scattered surface waves even at periods longer than 1 s at least up to 15 s. Consequently, we could examine the envelope characteristics before and after the ScS arrivals as a good indicator to measure the average strength of medium heterogeneity in the mantle region. There is significant frequency dependence such as the change of coda decay gradient associated with the ScS arrival becomes smaller as the period becomes shorter (Fig. 2). It might mean that we could resolve the dimension of the lower mantle heterogeneity using spectral analysis for the seismogram envelopes in the period band between 1 and 20 s.

To quantitatively analyze the envelopes characteristics around the ScS arrival, we adopted the DSMC method [12] based on the radiative transfer theory for isotropic scattering process and estimated the total scattering coefficient for 4 and 10 s period bands for the lithosphere and the upper mantle and for the lower mantle. We used the PREM model as a reference structure for velocity and total S-wave attenuation. In the total scattering coefficient of a wide period range over the world (Fig. 7), our results range the intermediate part between those for S-waves in the lithosphere with periods smaller than 1 s and that for Rayleigh waves in the lithosphere and the most upper mantle with periods larger than 100 s [22], and Lee et al. [11] obtained the value ranging from $10^{-5}$ to $10^{-4}$ $km^{-1}$ for the lower mantle at 4 and 10 s period bands in central Asia. We believe that the scattering coefficients estimated in this study are reliable especially for understanding the medium heterogeneity of the lower mantle. The resultant total scattering coefficients correspond to the mean free paths of about 1600–4800 km and 3700–36,000 km for the lower mantle at 4 and 10 s, respectively. The values for 4 s are roughly comparable to the result predicted by Shearer and Earle [9] examining at high frequencies (~1 Hz).

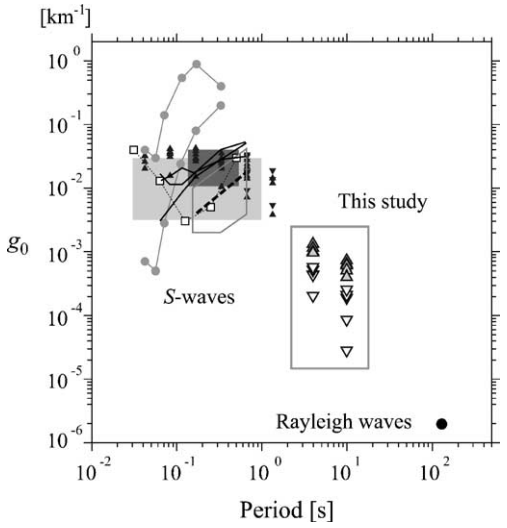


Fig. 7. Estimated total scattering coefficient of S-waves in the mantle from the analysis of ScS phase observed in 9 IRIS seismic stations are marked by triangles and inverted triangles within the open square region for Layer 1 (lithosphere and upper mantle) and Layer 2 (lower mantle), respectively. Total scattering coefficients of S-waves for short periods in the lithosphere [1] and those of Rayleigh waves for the lithosphere and the most upper mantle [22] are also plotted.

Fig. 8 represents the spatial distribution of the total scattering coefficients for the lithosphere and the upper mantle and for the lower mantle regions. In particular, some regional differences of the lower mantle heterogeneity appear as strong scattering beneath central Asia for 4 and 10 s and Papua New Guinea for 4 s, and weak scattering beneath Italy and regions of east Russia for 10 s. Although there is also significant strong scattering beneath YSS for 4 s and LPAZ for 10 s, the total scattering coefficients might be not reliably resolved at the regions considering relatively larger residual. Except for them, the result shows good correlation with the image of scattering strength for the mantle over the world [6,23].

The radiative transfer theory provides a method for distinguishing scattering attenuation from intrinsic absorption by analyzing the entire S-wave seismogram. Reported ratios of scattering loss to total attenuation, known as seismic Albedo ($B_0$), range from 30% to 80% in the frequency band 1–20 Hz using a model based on isotropic scattering for the lithosphere. In this study, the

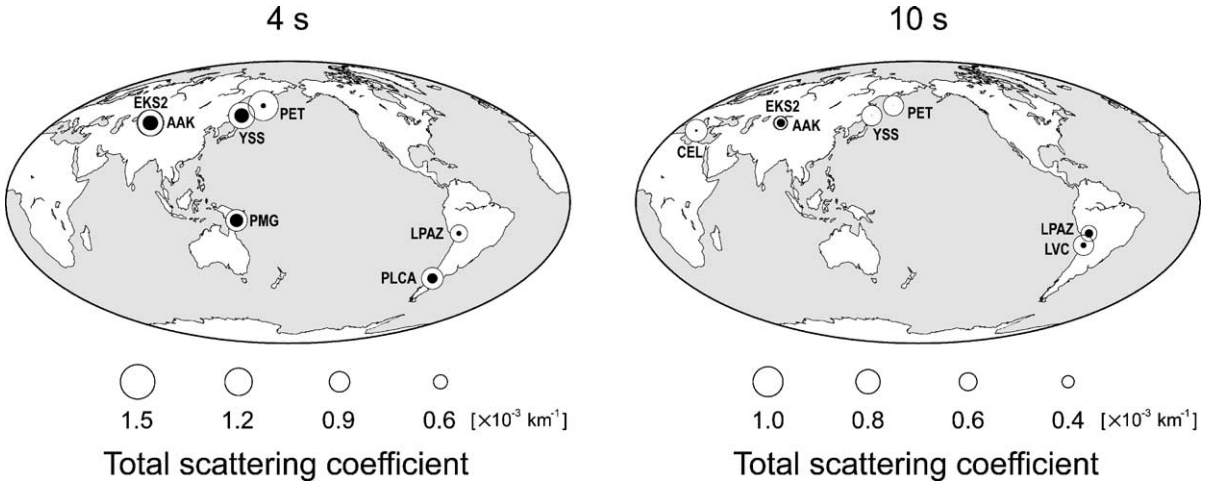


Fig. 8. Spatial variation of the total scattering coefficients for the lithosphere and the upper mantle and for the lower mantle. The size of circles corresponds to the strength of medium heterogeneity. Open and solid circles represent the values for Layer 1 (lithosphere and upper mantle) and Layer 2 (lower mantle), respectively.

seismic Albedo in the lower mantle for the periods of 4 and 10 s are higher than 64% beneath Kyrgyzstan in central Asia and Papua New Guinea in south-west Pacific, which show the high level of coda excitation with significant gradient change around the ScS arrival. It tells us that the scattering mechanism mainly controls the seismic attenuation when the seismic waves pass through the lower mantle beneath the regions. Therefore, beneath central Asia and south-west Pacific, much stronger scattering than intrinsic attenuation might cause the offset behavior and coda decay gradient change after the ScS arrival for 4 and 10 s period bands.

In addition to S-wave scattering especially before the ScS arrival, we need to note a contribution of surface wave scattering. This suggests that the study of the mantle heterogeneity requires the scattering, reflection, and conversion of the surface waves at the mantle discontinuities to measure the spatial variation of mantle heterogeneity. The depth profile and spatial variation of S-wave scattering coefficient enables us to understand the scattering and the attenuation processes more quantitatively not only in the lithosphere but also deep in the mantle.

## 6. Conclusions

We have examined the characteristics of seismic envelopes for the deep focus ($\geq 150$ km) regional earthquakes recorded 9 IRIS seismic stations in periods from 1 to 20 s for a wide lapse time range up to 2000 s, and found significant frequency dependence such as the coda decay gradient at short periods is steeper than that at longer periods; however, the change of coda gradient associated with the ScS arrival becomes distinct as the period becomes longer. In particular, clear offset with coda gradient change appears in central Asia for 10 and 15 s period bands. Grid search analysis applying the DSMC method for synthesizing S-wave envelopes used our two-plane-layer attenuation model yields quite reasonable total scattering coefficients for the lower mantle at 4 and 10 s. That is, our results maintain that medium heterogeneity spreads over the whole mantle though its scattering power is small, the model of whole-mantle heterogeneity. The estimated total scattering coefficients for Layer 1 (lithosphere and upper mantle) and Layer 2 (lower mantle) are $7.52\times10^{-4}$~$1.32\times10^{-3}$ $km^{-1}$ (for $\pm$20% in error) and $2.08\times10^{-4}$~$6.23\times10^{-4}$ $km^{-1}$ (for $\pm$20% in error) at 4 s, and $4.51\times10^{-4}$~$7.37\times10^{-4}$ $km^{-1}$ (for $\pm$10% in error) and $2.80\times10^{-5}$~$2.71\times10^{-4}$ $km^{-1}$ (for $\pm$10% in error) at 10 s, respectively. The results indicate particularly strong scattering beneath central Asia at 4 and 10 s and Papua New Guinea at 4 s, whereas weak scattering is obtained beneath Italy and regions of east Russia at 10 s for the lower mantle. Much stronger scattering than intrinsic attenuation in the lower mantle causes the offset behavior with the change of coda decay gradient after the ScS arrival for 4 and 10 s period bands in some regions.

## Acknowledgements

The authors would like to thank R. D. van der Hilst, M. Fehler and an anonymous reviewer for their helpful comments on the manuscript. The data used in this research were acquired by high-quality data in the

FARM archive at the IRIS DMC. This research has been supported by a grant to W. S. Lee (JSPS Postdoctoral Fellowship of Japan and BK21 Project of Korea). Some of maps were produced using GMT.

## References

[1] H. Sato, M.C. Fehler, Seismic wave propagation and scattering in the heterogeneous earth, AIP Press/Springer Verlag, New York, 1998, 308 pp.
[2] T.G. Rautian, V.I. Khalturin, The use of the coda for determination of the earthquake source spectrum, Bull. Seismol. Soc. Am. 68 (1978) 923–948.
[3] N.N. Biswas, K. Aki, Characteristics of coda waves: central and south central Alaska, Bull. Seismol. Soc. Am. 74 (1984) 493–507.
[4] H. Sato, M. Nohechi, Envelope formation of long-period Rayleigh waves in vertical component seismograms: single isotropic scattering model, J. Geophys. Res. 106 (2001) 6589–6594.
[5] M.A.H. Hedlin, P.M. Shearer, P.S. Earle, Seismic evidence for small-scale heterogeneity throughout the Earth's mantle, Nature 387 (1997) 145–150.
[6] M.A.H. Hedlin, P.M. Shearer, An analysis of large-scale variations in small-scale mantle heterogeneity using Global Seimographic Network recordings of precursors to PKP, J. Geophys. Res. 105 (2000) 13655–13673.
[7] L. Margerin, G. Nolet, Multiple scattering of high-frequency seismic waves in the deep Earth: modeling and numerical examples, J. Geophys. Res. 108 (2003) 2234, doi:10.1029/2002JB001974.
[8] L. Margerin, G. Nolet, Multiple scattering of high-frequency seismic waves in the deep Earth: PKP precursor analysis and inversion for mantle granularity, J. Geophys. Res. 108 (2003) 2514, doi:10.1029/2003JB002455.
[9] P.M. Shearer, P.S. Earle, The global short-period wavefield modeled with a Monte Carlo seismic phonon method, Geophys. J. Int. 158 (2004) 1103–1117, doi:10.1111/j.1365-246X.2004.02378.x.
[10] P.S. Earle, P.M. Shearer, Distribution of fine-scale mantle heterogeneity from observations of $P_{diff}$ coda, Bull. Seismol. Soc. Am. 91 (2001) 1875–1881.
[11] W.S. Lee, H. Sato, K. Lee, Estimation of S-wave scattering coefficient in the mantle from envelope characteristics before and after the ScS arrival, Geophys. Res. Lett. 30 (2003) 2248, doi:10.1029/2003GL018413.
[12] K. Yoshimoto, Monte Carlo simulation of seismogram envelopes in scattering media, J. Geophys. Res. 105 (2000) 6153–6161.
[13] B.L.N. Kennett, E.R. Engdahl, Travel times for global earthquake location and phase association, Geophys. J. Int. 105 (1991) 429–465.
[14] N. Bellomo, L. Arlotti, Lecture Notes on the Mathematical Theory of the Boltzmann Equation, World Scientific Publishing Company, New Jersey, 1995, 255 pp.
[15] M. Hoshiba, Seismic coda wave envelope in depth-dependent S wave velocity structure, Phys. Earth Planet. Inter. 104 (1997) 15–22.
[16] A.M. Dziewonski, D.L. Anderson, Preliminary reference Earth model, Phys. Earth Planet. Inter. 25 (1981) 297–356.
[17] A.A. Gusev, I.R. Abubakirov, Vertical profile of effective turbidity reconstructed from broadening of incoherent body-wave pulses-II. Application to Kamchatka data, Geophys. J. Int. 136 (1999) 309–323.
[18] H. Sato, M. Fehler, T. Saito, Hybrid synthesis of scalar wave envelopes in two-dimensional random media having rich short wave-length spectra, J. Geophys. Res. 109 (2004) B06303, doi:10.1029/2003JB002673.
[19] M. Hoshiba, Simulation of coda wave envelope in depth dependent scattering and absorption structure, Goephys. Res. Lett. 21 (1994) 2853–2856.
[20] A.A. Gusev, Vertical profile of turbidity and coda $Q$, Geophys. J. Int. 123 (1995) 665–672.
[21] K. Aki, B. Chouet, Origin of coda waves: source, attenuation and scattering effects, J. Geophys. Res. 80 (1975) 3322–3342.
[22] H. Sato, M. Nishino, Multiple isotropic-scattering model on the spherical Earth for the synthesis of Rayleigh-wave envelopes, J. Geophys. Res. 107 (2002) 2343–2351.
[23] J.E. Vidale, M.A.H. Hedlin, Evidence for partial melt at the core–mantle boundary north of Tonga from the strong scattering of seismic waves, Nature 391 (1998) 682–685.